LUMIO: A CUBESAT AT EARTH-MOON L2

F. Topputo [1], M. Massari [1], J. Biggs [1], P. Di Lizia [1], D. Dei Tos [1], K. Mani [1], S. Ceccherini [1], V. Franzese [1], A. Cervone [2], P. Sundaramoorthy [2], S. Speretta [2], S. Mestry [2], R. Noomen [2], A. Ivanov [3], D. Labate [4], A. Jochemsen [5], R. Furfaro [6], V. Reddy [6], K. Jacquinot [6], R. Walker [7], J. Vennekens [7], A. Cipriano [7],

[1] Politecnico di Milano, Via La Masa 34, 20156, Milano, Italy
[2] TU Delft, Kluyverweg 1, 2629, Delft, The Netherlands
[3] École Polytechnique Fédérale de Lausanne, Route Cantonale, 1015, Lausanne, Switzerland
[4] Leonardo, Via delle Officine Galileo 1, 50013, Campi Bisenzio, Florence, Italy
[5] Science and Technology AS, Tordenskiolds Gate 3, 0160, Oslo, Norway
[6] University of Arizona, 1130 N Mountain Ave., 85721, Tucson, AZ, United States
[7] ESA/ESTEC, Keplerlaan 1, 2201 AZ, Noordwijk, The Netherlands

ABSTRACT

The Lunar Meteoroid Impact Observer (LUMIO) is a CubeSat mission to observe, quantify, and characterize the meteoroid impacts by detecting their flashes on the lunar farside. LUMIO is one of the two winners of ESA's LUCE (Lunar CubeSat for Exploration) SYSNOVA competition, and as such it is being considered by ESA for implementation in the near future. The mission utilizes a CubeSat that carries the LUMIO-Cam, an optical instrument capable of detecting light flashes in the visible spectrum. On-board data processing is implemented to minimize data downlink, while still retaining relevant scientific data. The mission implements a sophisticated orbit design: LUMIO is placed on a halo orbit about Earth–Moon L2 where permanent full-disk observation of the lunar farside is made. This prevents background noise due to Earthshine, and permits obtaining high-quality scientific products. Innovative full-disk optical autonomous navigation is proposed, and its performances are assessed and quantified. The spacecraft is a 12U form-factor CubeSat, with 22 kg mass. Novel on-board micro-propulsion system for orbital control, de-tumbling, and reaction wheel desaturation is used. Steady solar power generation is achieved with solar array drive assembly and eclipse-free orbit.

1 SCIENCE

1.1 Relevance

Impacts due to near Earth objects could cause a devastating humanitarian crisis and potentially the extinction of the human race. While the probability of such an event is low, the outcome is so catastrophic that it is imperative to invest resources to mitigate them. Telescopic surveys detect NEOs > 1 km down to 1 meter, but there are few direct methods for monitoring the sub-meter meteoroid population. Serendipitous monitoring of atmospheric explosions due to airbursts of meteoroids are being undertaken. These objects are part of the ~33 metric tons of debris impacting the Earth each day.

Meteoroids are small Sun-orbiting fragments of asteroids and comets, whose sizes range from micrometers to meters and masses from 10^{-15} to 10^{4} kg [1]. Their formation is a consequence of asteroids colliding with each other or with other bodies, comets releasing dust particles when close to the Sun, and minor bodies shattering into individual fragments. Meteoroids are hardly detectable

even with dedicated surveys. However, they may be observed indirectly when an impact occurs with a planetary or moon solid surface. An impact represents in fact a unique opportunity to understand and update the models describing the spatial distribution of NEOs in the solar system, which is critical for several reasons. The ability to accurately and timely predicting these impacts by relying on accurate meteoroid impact flux models is fundamental in many fields.

1.2 Lunar meteoroid impacts

Current estimations of the larger-than-1-kg meteoroid flux at the Moon varies across the literature. The model in [2] estimates 1290 impacts per year, while the one in [3] estimates approximately 4000 impacts per year [4]. More recent studies suggest that the meteoroid impact flux at the Moon is approximately 6 10^{-10} m^2/year, for meteoroids larger than 30 grams [5]. Assuming a lunar collecting area equal to its surface area, 3.8 10^{13} m^2, this gives a larger-than-30-grams meteoroid flux of approximately 23,000 impacts per year.

There are also speculations on the possible asymmetries of the spatial distribution of impacts across the lunar surface. In [6], it is theorized that the Moon nearside has approximately 0.1% more impacts than the lunar farside, due to the Earth gravity field; the equatorial flux is 10–20% larger than that at polar regions, due to the higher number of large meteoroids in low orbital inclinations; and the lunar leading side (apex) encounters between 37% to 80% more impactors than the lunar trailing side (antapex), due the Moon synchronous rotation.

In a lunar meteoroid impact, the kinetic energy of the impactor is partitioned into 1) the generation of a seismic wave, 2) the excavation of a crater, 3) the ejection of particles, and 4) the emission of radiation. Any of these phenomena can be observed to detect lunar meteoroid impacts. The detection of lunar impact flashes is the most advantageous method since it yields an independent detection of meteoroid impacts, provides the most complete information about the impactor, and allows for the monitoring of a large Moon surface area. Remote observation of light flashes is thus baselined for the detection of lunar meteoroid impacts.

1.3 Sun-Earth-Moon Geometry

The Moon spin–orbit motion is locked into a 1:1 resonance, meaning that an observer on Earth always sees the same portion of the Moon, that is, the lunar nearside. This characteristic, in addition to the fact that a fixed observer on Earth also moves with respect to the Moon, as the Earth rotates about its own axis, constrain the observation of the Moon from the Earth.

Since the Moon–Sun synodic period is 29.53 days, the illumination of the lunar nearside varies, which originates the Moon phases. Because lunar impact flashes can only be observed from ground on the lunar nightside and when the lunar nearside is less than 50% illuminated, their detection from Earth is constrained by this Sun–Earth–Moon geometry. It should be noted that an observer of the lunar farside would also be constrained by the Sun–Moon geometry, but would see temporally opposite phases. As such, assuming that the lunar farside would also have to be less than 50% illuminated, the observations would occur during the opposite time of the month (Figure 1).

Observing the lunar impacts with space-based assets yields a number of benefits over ground-based telescopes, namely:

- *No atmosphere*. Ground-based observations are biased by the atmosphere that modifies (reduces) the light flash intensity depending upon present conditions, which change in time. This requires frequent recalibration of the telescope. Inherent benefits of the absence of atmosphere in space-based observations are twofold: 1) there is no need of recalibrating the instrument, and 2) fainter flashes can be detected.
- *No weather*. Ground-based observations require good weather conditions, the lack of which may significantly reduce the observation time within the available window. There is no such constraint in space-based observations.
- *No day/night*. Ground-based observations may only be performed during Earth night,

significantly reducing the observation period within the available window. There is no such limitation when space-based observations are performed.

- *Full disk*. Ground-based observations are performed in the first and third quarter, when nearside illumination is 10–50%. Full-disk observations during New Moon are not possible because of low elevation of the Moon and daylight. Space-based observations of the lunar farside can capture the whole lunar full-disk at once, thus considerably increasing the monitored area.
- *All longitudes*. Ground-based observations happening during the first and third quarter prevent resolving the meteoroid flux across the central meridian. There is no such restriction in space-based, full-disk observations.

Moreover, observing the lunar farside with space-based assets yields further benefits, that is:

- *No Earthshine*. By definition, there is no Earthshine when observing the lunar farside. This potentially yields a lower background noise, thus enabling the detection of fainter signals, not resolvable from ground.
- *Complementarity*. Space-based observations of the lunar farside complement ground-based ones
  - In space: The two opposite faces of the Moon are monitored when the Moon is in different locations along its orbit;
  - In time: Space-based observations are performed in periods when ground-based ones are not possible, and vice-versa.

High-quality scientific products can be achieved with *space-based observations of the lunar farside*. These may complement those achievable with ground-based ones to perform a comprehensive survey of the meteoroid flux in the Earth–Moon system.

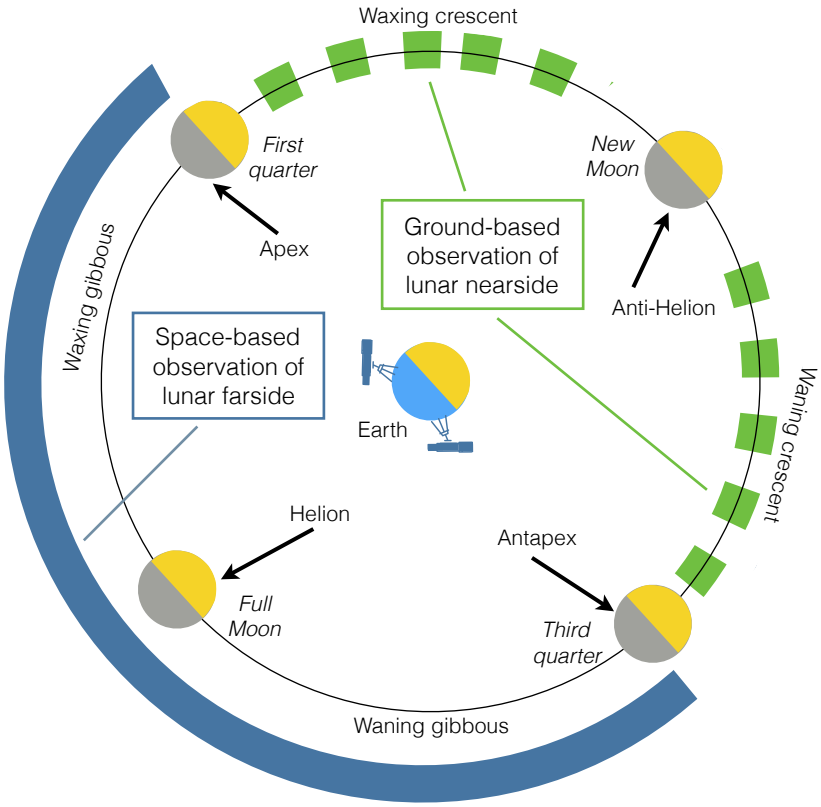

Figure 1. Moon phases and main directions of incoming meteoroids in the Earth-Moon system (North and South Toroidal sources are perpendicular to the plane). The dashed green line represents the portion of the Moon orbit where Earth-based observations of the nearside can be made. The solid blue line indicates the portion of the Moon orbit where space-based observations of the farside can be made.

1.4 Lunar Meteoroid Impact Flash Detection

Light flashes at the Moon are typically observed by detecting a local spike of the luminous energy in the visible spectrum when pointing a telescope at the lunar nightside. The background noise is mainly composed by the Earthshine (Earth reflected light on the Moon surface) in the visible spectrum, and by thermal emissions of the Moon surface in the infrared spectrum [7]. Measurements with high signal-to-noise ratios can be obtained through observations of the lunar nightside [8]. The detected luminous energy spike is quantified using the apparent magnitude of the light flash.

Lunar impact flashes detected from Earth-based observations have apparent magnitude between +5 and +10.5 [6], which correspond to very faint signals. Also, Earth-based observations of lunar impact flashes are restricted to periods when the lunar nearside illumination is 10–50% [3], [9]. The upper limit restriction is due to the dayside of the Moon glaring the telescope field of view (FOV). The lower limit restriction of 10\% corresponds to the New Moon phase. During this phase, the observations should be made when the Moon presents itself at low elevations in the sky (morning or evening), but the observation periods are too short to be useful [6], [9].

The first unambiguous lunar meteoroid impact flashes were detected during 1999's Leonid meteoroid showers and were reported in [8]. The first redundant detection of sporadic impacts was only reported six years later in [3]. These events gave origin to several monitoring programs. In 2006, a lunar meteoroid impact flashes observation programme was initiated at NASA Marshall Space Flight Center [9]. This facility can monitor 4.5 10^6 km^2 of the lunar surface, approximately 10 nights per month, subject to weather conditions. Approximately half of the impact flashes observations occur between the Last Quarter and New Moon (0.5 to 0.1 illumination fraction) and the other half between New Moon and First Quarter (0.1 to 0.5 illumination fraction). The former monitoring period occurs in the morning (waning phase) and the latter occurs in the evening (waxing phase), covering the nearside part of the eastern and western lunar hemisphere, respectively. 126 high-quality flashes were reported in [5], for 266.88 hours of monitoring, over a 5 years period. The magnitude range detected is between +10.42 and +5.07, which is estimated to correspond to an impactor kinetic energy range between 1.67 10^{-7} and 2.31 10^{-4} kton TNT. The most recent monitoring program, NELIOTA, was initiated on February 2017 in Greece under ESA funding. As of November 2017, 16 validated impacts have been detected over 35 hours of observations. The program aims to detect flashes as faint as +12 apparent visual magnitude [10] and is the first allowing the determination of the impact flash blackbody temperature, by observing both in the visible and infrared spectrum. Monitoring the Moon for impact flashes inherently imposes several restrictions that can be avoided if the same investigation is conducted with space-bases assets.

1.5 LUMIO mission

LUMIO is a CubeSat mission to a halo orbit at Earth–Moon L_2 that shall observe, quantify, and characterize meteoroid impacts on the lunar farside by detecting their impact flashes, complementing Earth-based observations on the lunar nearside, to provide global information on the lunar meteoroid environment and contribute to Lunar Situational Awareness.

LUMIO mission is conceived to address the following issues.

- *Science Question*: What are the spatial and temporal characteristics of meteoroids impacting the lunar surface?
- *Science Goal*. Advance the understanding of how meteoroids evolve in the cislunar space by observing the flashes produced by their impacts with the lunar surface.
- *Science Objective*. Characterize the flux of meteoroids impacting the lunar surface.

2 PAYLOAD

The observation of the light flashes produced by meteoroid impacts on the Moon far-side is performed through the LUMIO-Cam, the main payload of the LUMIO CubeSat.

2.1 Payload Requirements

The impact flashes on the Moon can be modelled as black body emissions [6], with temperatures between 2700 K and 6000 K [7], and durations greater than 30 ms [5]. The lowest impact energies correspond to apparent magnitudes higher than 6 as seen from Earth. These characteristics drive the payload requirements, which are listed in Table 1. The camera detection and optics are guided by requirements PLD.001 to PLD.003, while requirements PLD.004 to PLD.007 constrain the payload physical properties in terms of total mass, volume, power consumption, and storage, due to the need of compliance with low-resource CubeSat standards.

Table 1. LUMIO payload requirements.

ID	Requirement
PLD.001	The payload shall detect flashes with energies between 10^{-6} and 10^{-1} kT TNT.
PLD.002	The payload shall detect flashes in the radiation spectrum between 450 nm and 890 nm.
PLD.003	The image integration time shall be equal or greater than 30 ms.
PLD.004	The mass of the payload shall be no more than 4.5 kg.
PLD.005	The maximum power consumption of the payload shall be no more than 10 W.
PLD.006	The maximum size of the payload shall be 10 cm x10 cm x 30 cm.
PLD.007	The payload processor shall create less than 20 MB of the science data per day.

2.2 Detector

The baseline detector is the CCD201 of E2V L3Vision™ . This device is a 1024x1024 pixel frame-transfer sensor that uses a novel output arrangement, capable of operating at an equivalent output noise of less than one electron at pixel rates of over 15 MHz. This makes the sensor well-suited for scientific imaging where the illumination is limited and the frame rate is high, as it is for LUMIO. The sensitivity of this detector extends towards the NIR region, which allows to better exploit the emission of radiation due to the impacts. The detector features are reported in Table 2.

Table 2. Detector features.

Parameter	Value	Parameter	Value
Image Area	13.3 mm x 13.3 mm	Low Noise Gain	1 – 1000
Active Pixels	1024 x 1024	Readout Frequency	15 MHz
Pixel Size	13.3 µm x 13.3 µm	Charge Handling Cap.	80ke$^-$/pixel
Storage Area	13.3 mm x 13.3 mm	Readout Noise	< 1 e$^-$ rms

2.3 Optics

Considering the LUMIO orbit, for which the S/C-Moon range spans between 35000 and 85000 km, a minimum payload field of view (FOV) of 5.68 deg is necessary to have always the Moon full disk view. To compensate for pointing errors and other effects, a 6 deg FOV is considered, leading to a 127 mm focal length. The LUMIO-Cam optics features are shown in Table 3.

Table 3. Optics features.

FOV	Focal Length	Aperture	F#
6.0 degrees	127 mm	55 mm	2.3

2.4 Mechanical Layout

The mechanical layout of LUMIO-Cam shown in Figure 2, and it includes a mechanical barrel supporting five lenses, an entrance baffle for out-of-field straylight reduction, a focal plane assembly, a proximity electronics box, and an external box for mechanical protection.

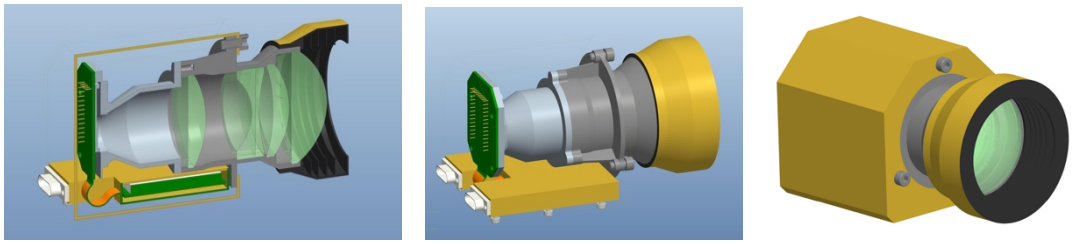

(a) **(b)** **(c)**

Figure 2. LUMIO-Cam Assembly; (a-b) Opto-Mechanical Assembly; (c) External Box .

2.5 Budgets

The mass and power budgets are reported in Table 4 and Table 5, where a 20% margin has been considered owing to the early stage of the design. The LUMIO-Cam total margined mass is 1.56 kg and its worst-case power consumption (margined) is 4.2 W.

Table 4. Payload mass budget.

	Mass [kg]	Margin [%]	Margined Mass [kg]
Lenses	0.3	20	0.36
Barrel	0.4	20	0.48
Baffle	0.1	20	0.12
Electronics	0.2	20	0.24
Box	0.3	20	0.36
Total	1.3	20	**1.56**

Table 5. Payload power budget.

	Power (Peek) [W]	Margin [%]	Margined Power [W]
Detector	0.2	20	0.24
TEC	2.3 (2.8)	20	2.76 (3.36)
Electronics	0.5	20	0.6
Total	3.0 (3.5)	20	**3.6 (4.2)**

2.6 Radiometric Analysis

A radiometric analysis employing the LUMIO-Cam properties has been performed to assess the capability of the payload to detect the phenomenon under study. The detector collects photons emitted by the impact flash, but also some undesired signals, which are considered as noise (e.g., the straylight background noise, the dark current, the CCD's ReadOut Noise, etc.).
The Signal-to-Noise Ratio (SNR), output of the radiometric analysis, is always higher than 5 dB, assuring the detectability of the entire range of meteoroids impact energies.

2.7 On-board Payload Data Processing

On-board image processing is required due to the high amount of data generated by the payload. For an acquisition rate of 1.8 MB images at 15 fps, the data products of the payload would be around 2.4 TB/day of science acquisitions. To reduce this amount, the OBPDP detects flashes in the images and stores only the images with scientific relevance. This leads to a reduction by a factor of 23000. Since not all pixels of the full frame image are scientifically relevant data, the OBPDP will also cut away everything outside an area around the flash. In this way, from 35.7 TB gathered during a LUMIO orbit period (14.7 days), just 13 Mb of data needs to be stored (Figure 3).

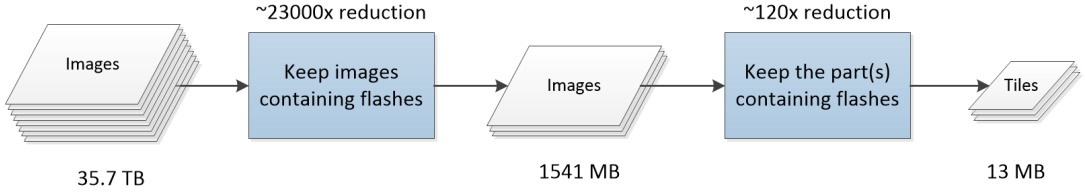

Figure 3: Data amount reduction.

3 MISSION ANALYSIS

It has been shown that remotely detecting flashes is the only technically and economically viable option for a CubeSat to monitor meteoroid impacts on the lunar surface. When considering the conclusions in [11] of the preliminary and coverage trade-offs, the mission type flight heritage, and solar eclipse occurrences, the **Earth–Moon L2 halo family is baselined for LUMIO mission**. The vertical Lyapunov orbit family is selected as back-up plan and it is not detailed in this paper.

The LUMIO mission is divided in 4 well defined phases (refer to Figure 4),

1. Parking:
    a. Starts when the lunar orbiter deploys LUMIO on the prescribed selenocentric elliptic parking orbit;
    b. Ends when LUMIO performs the Stable Manifold Injection Maneuver (SMIM);
    c. Lasts 14 days.
2. Transfer:
    a. Starts when LUMIO completes the SMIM;
    b. Ends when LUMIO performs the Halo Injection Maneuver (HIM); c. Lasts 14 days.
3. Operative:
    a. Starts when LUMIO completes the HIM;
    b. The primary mission modes during the operative phase are Science Mode and Navigation and Engineering Mode (or Nav&Eng), that alternate between every other orbit;
    c. Ends after one year of operations.
4. End of Life (EoL):
    a. Starts with de-commission of all (sub)systems;
    b. Ends when the EoL maneuver is correctly performed for safe disposal of the spacecraft.

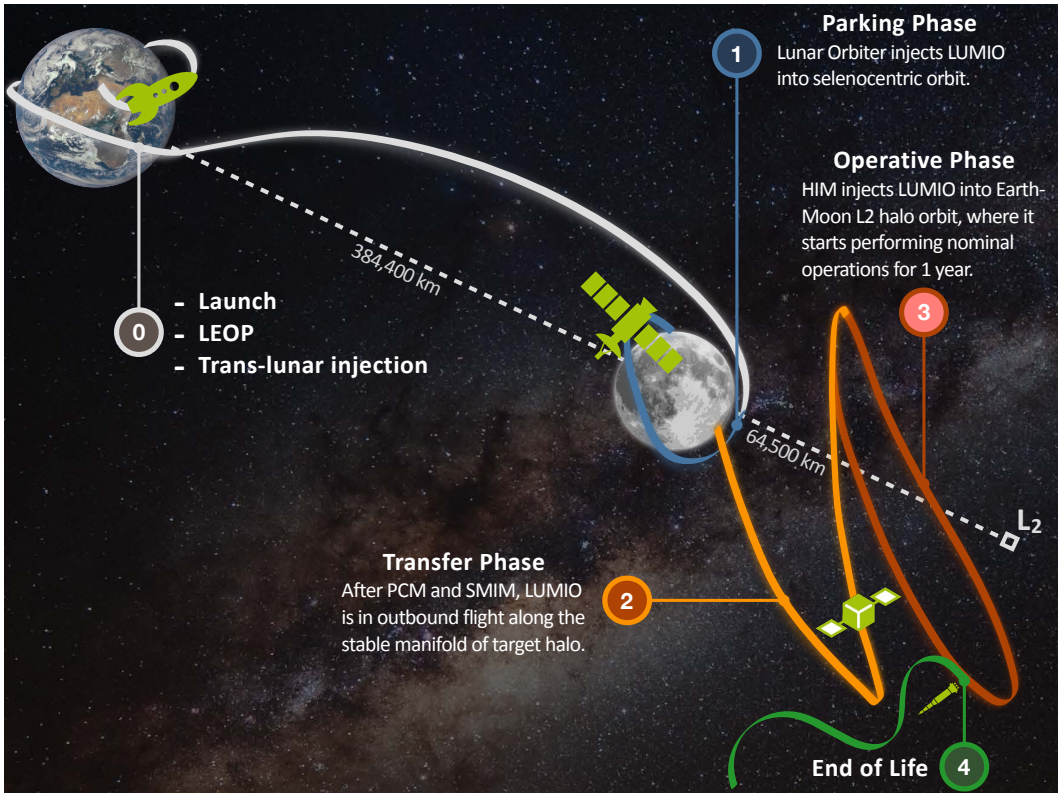

Figure 4. Sketch of LUMIO mission phases.

3.1 Earth--Moon L_2 quasi-halos in high-fidelity model

A set of quasi-periodic halo orbits (sometimes referred here as quasi-halos or quasi-halo orbits) about Earth--Moon L_2 are found by employing the methodology described in [12]. Fourteen quasi-halo orbits are computed in the high-fidelity roto-pulsating restricted *n*-body problem (RPRnBP) and saved as SPICE[1] kernels. The initial feeds to compute the quasi-halo samples are Earth--Moon three-body halos at 14 different Jacobi constants, ranging from $C_j = 3.04$ to $C_j = 3.1613263$. The latter value corresponds to the one assumed for the very first iteration of the activities. All orbits are computed starting from 2020 August 30 00:00:00.00 TDB. Although quasi-halos, shown in Figure 5, are computed for a fixed initial epoch, the persistence of libration point orbits in the solar system ephemeris model allows wide freedom in the refinement algorithm, which also includes mission starting at different epochs [13].

Quasi-halo orbits of Figure 5 are all possible LUMIO operative orbits. As the orbit becomes more energetic (or as its CRTBP Jacobi constant decreases), the quasi-halo exhibits a wider range of motion both in terms of a) Moon range and of b) geometrical flight envelope about the corresponding CRTBP trajectory. The latter trend is disadvantageous when a hard-pointing constraint must be respected (e.g., Moon full disk on optical instrument). On the other hand, the lunar distance places a constraint on the minimum FOV for the optical instrument on board LUMIO to be able to resolve the Moon full disk at any location along the quasi-halo.

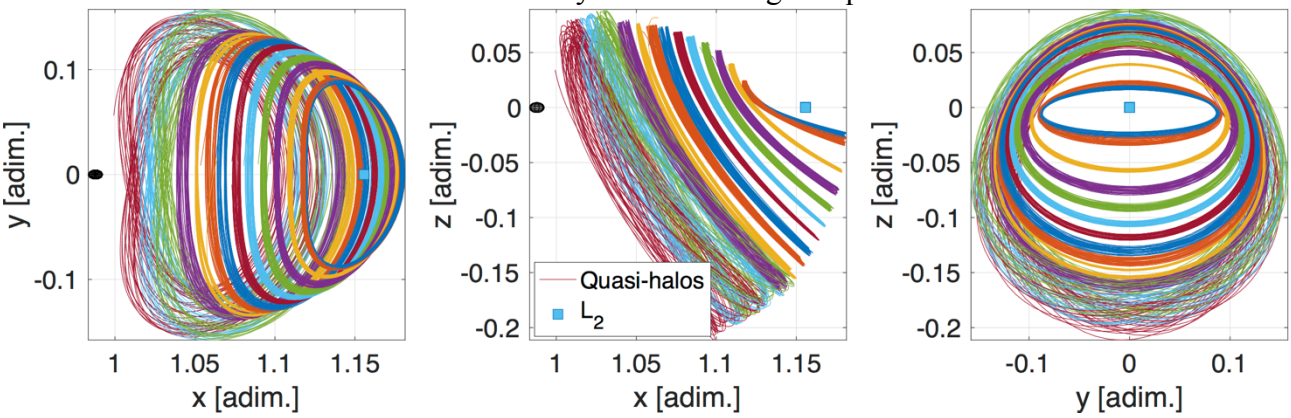

Figure 5 Projection of Earth--Moon L_2 quasi-halos in the roto-pulsating frame.

3.2 Orbital transfer to quasi-halo orbit

The transfer phase of LUMIO is done entirely in the CRTBP. Free transport mechanisms are leveraged to reach a target halo. Specifically, intersection in the configuration space is sought between the halo stable manifolds and a selenocentric transition orbit. Since the sought intersection occurs only in configuration space, a maneuver is necessary for orbital continuity. This maneuver places the spacecraft on the stable manifold of the target halo and is thus called stable manifold injection maneuver (SMIM), Δv_{SMIM}. The transfer phase starts when the SMIM is executed, and ends after the halo injection maneuver (HIM), Δv_{HIM}, inserts the S/C into the target halo orbit. The aim of the transfer design analysis is to find the parameters of the selenocentric transition orbit and the stable manifold that lead to a minimum Δv_{SMIM} at the intersection. The optimization problem is stated as a NLP method and then solved with the Matlab active-set algorithm. The transfer parameters to quasi-halo generated by $C_j = 3.09$ are shown in Table 6. As expected, the SMIM occurs at the periselene of the transition orbit (i.e., $\theta \cong 0$). The inclination of the transition orbit lies within the parking orbit bounds, and no plane maneuver is necessary.

Table 6. Main parameters for the transfer phase.

Parameter	h_p(km)	h_a(km)	i (deg)	Ω(deg)	ω(deg)	θ(deg)	T (hrs)	t_{po} (-)	t_{sm} (-)
Value	200	14,964.2	78.1	30.0	301.2	~0	22.42551	0.7406	7.5397

[1] SPICE is NASA's Observation Geometry and Information System for Space Science Missions [19], [20]. The toolkit is freely available through NASA NAIF website (last accessed on February 7, 2018).

3.3 Station-keeping on quasi-halo orbit

In light of the limited Δv capability, fuel consumption for station-keeping around the operative orbits will be a critical factor for mission sustainability. Taking advantage of the generated orbits as reference trajectories, an effort is directed toward the development of a station-keeping strategy that can be used to maintain CubeSats near such nominal LPOs. The S/K cost is estimated by employing the *target points method* (TPM) first introduced in [14], then adapted to the problem of LPOs by [15], and finally used for JAXA's EQUULEUS mission analysis [16]. A massive Monte-Carlo simulation is performed with 10,000 samples, considering the impact of the injection, tracking, and maneuver execution processes on the nominal orbit determined in the presence of solar radiation pressure and gravity of the main solar system celestial bodies (i.e., Sun, 8 planets, the Moon, and Pluto). The errors on orbit injection, orbit determination, and the maneuver execution are all modeled and generated with zero-mean Gaussian distributions, where position, velocity, and maneuver offset covariances are set to 10 km, 10 cm/s, and 2%, respectively. This is compliant with navigation performances [17]. The TPM parameters and the S/K maneuvers epochs are fine-tuned for the LUMIO specific quasi-halos application with a direct simulation technique.

Table 7 displays the 1-year S/K cost with 1σ, 2σ, and 3σ confidence. The Monte-Carlo data is fitted by means of an Inverse Gaussian distribution. As expected, the S/K cost increases for smaller (i.e., higher Jacobi constant) quasi-halos. This trend reflects the stability (eigenspectrum of monodromy matrix) properties of halo orbits. That is, a larger halo is generally less unstable and thus cheaper to maintain.

Table 7. Confidence for the 1-year station-keeping cost.

C_j [nondim]	S/K cost [m/s]		
	1σ	2σ	3σ
3.09	18.3	23.9	28.1

3.4 LUMIO operative orbit

Figure 6 shows the total transfer cost for different halos. The cost includes S/K, SMIM, and plane change maneuvers. It is conjectured the reason why the transfer cost has a clear-cut minimum area is twofold: 1) For high energy levels (i.e., low Jacobi constant), the stable manifold configuration space does not get close enough to the Moon to permit intersection with the selenocentric transition orbit; 2) at the other end of the spectrum, for high Jacobi constant values, the stable manifolds cross the lunar region sufficiently close to provide patching opportunities with a selenocentric transition orbit, but the speed mismatch is comparatively large, that is the outbound stable manifold is much faster than the S/C at periselene.

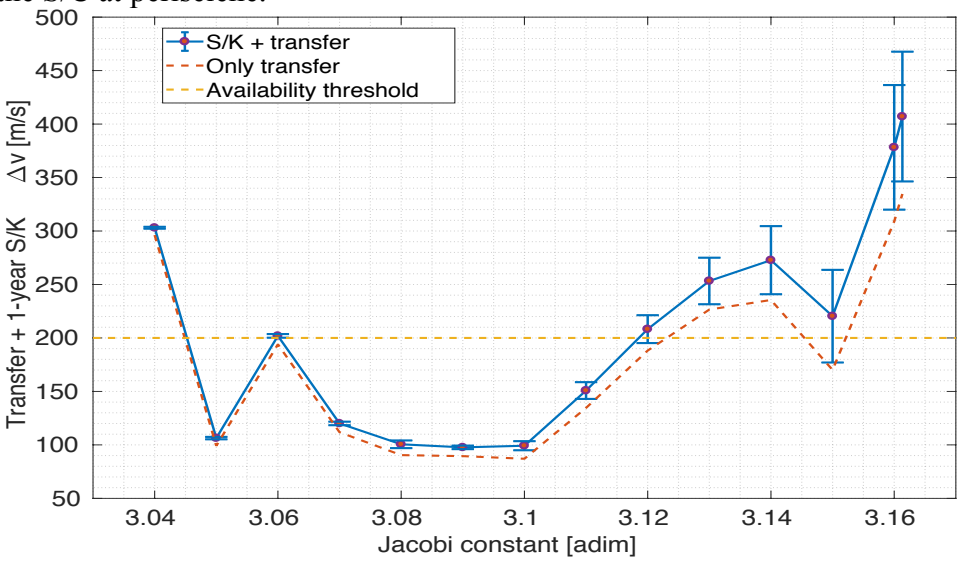

Figure 6. Total transfer cost for different halos.

Quasi-halo generated from C_j = 3.09 is the designated LUMIO operative orbit. The selection of LUMIO operative orbit is based on results of Figure 6. Indeed, the quasi-halo is located at the center of a minimum plateau for total transfer cost which provide both a) optimality of maneuvers cost, and b) robustness against errors in the actual energy level of the injected stable manifold.

Mission Δv budgets for each maneuver and phase are reported in Table 8 with both deterministic and confidence values. The 1σt is 154.4 m/s, which is also in line with a 12U CubeSat volume and mass budgets. Note that ESA "Margin philosophy for science assessment studies" (Ref. SRE-PA/2011.097/, item MAT-DV-14) states that stochastic maneuvers shall be calculated based on the 3σ confidence interval with no additional margins [18]. The choice to consider a 1σ confidence interval on stochastic maneuvers for LUMIO is motivated by the inherently higher risk of a low-cost mission. Nonetheless, the overall stochastic Δv computed based on a 95.32% confidence level of a combination of all stochastic maneuvers is smaller than linear sum by 19%. With this approach, the 3σ Δv budget sums up to 191.3 (195.5 with margins on SMIM, HIM, and disposal maneuver), which is still within the bounds for mission feasibility according.

Table 8 Mission Δv budgets.

Maneuver	Cost [m/s]			
	Deterministic	1σ	2σ	3σ
PCM	0	-	-	-
Transition orbit S/K	-	8	8	8
SMIM	89.47	-	-	-
TCM1	-	28.6	53.0	73.1
TCM2	-	6.5	15.0	24.8
HIM	0.5	-	-	-
1-year S/K	0	18.3	23.9	28.1
Disposal	3	-	-	-
TOTAL	154.4		192.9	227.0

4 SYSTEM

The LUMIO spacecraft has been designed to perform with a high level of autonomy, particularly the Navigation, Payload Data Processor and CDHS subsystems. This choice was driven not only by the operational constraints with respect to the Lunar orbiter, but also by the ambitious mission design. Additionally, a general zero-redundancy approach has been adopted for all subsystems. This is dictated by the tight mass and volume constraints and a CubeSat design driven risk approach.

In subsystem design, a systematic trade-off procedure has been adopted, based on subsystem specific performance criteria, as well as standard performance, cost and schedule criteria. Consistent design margins have been used for sizing the subsystems based on the development status. A standard 5, 10 and 20% mass margin has been applied for a fully COTS solution, a COTS solution requiring modification and a custom design, respectively.

The most important system and sub-system requirements are summarized in Table 9.

Table 9. Main system and subsystem requirements

OVRSYS-001	*The mass of the spacecraft shall be no greater than 24 kg*
OVRSYS-002	*The spacecraft volume shall not exceed that of a 12U CubeSat*
OVRSYS-003	*The system shall operate in a standalone mode for a period of 10 days without any communication*
PROP-001	*The propulsion system shall provide a minimum ΔV =154.39 m/s for station keeping, orbital transfer, end-of-life disposal, and a minimum total impulse of 72.91 Ns for de-tumbling and wheel desaturation maneuvers*
PROP-002	*The maximum thrust of the propulsion system shall be 500 mN*
PROP-003	*The propulsion system shall have maximum thrusting time of 8 hours per orbital transfer maneuver*
ADCS-001	*After the separation from the Lunar Orbiter, the ADCS shall de-tumble the spacecraft from tip-off rates of, up to 30 deg/s in each axis*

ADCS-003	*The ADCS shall point with an accuracy of less than 0.1 deg during science and navigation phases*
ADCS-005	*The ADCS shall provide minimum pointing stabilization of 79.90 arcsec/s during the science phase*
ADCS-006	*The ADCS shall provide a maximum slew rate of 1 deg/s*
EPS-002	*The EPS shall supply 22 W average and 36 W peak power to the subsystems in parking orbit phase*
EPS-004	*The EPS shall supply 23 W average and 39 W peak power to the subsystems during transfer phase*
EPS-006	*The EPS shall supply 27 W average and 46 W peak power to the subsystems in science mode*
EPS-008	*The EPS shall supply 22 W average and 42 W peak power to the subsystems in navigation mode*
EPS-013	*The EPS shall have a mass no more than 3 kg*
COMMS-001	*The spacecraft shall receive Telecommands from Lunar Orbiter at frequency range 390-405 MHz*
COMMS-002	*The spacecraft shall send Telemetry to the Lunar Orbiter at frequency range 435-450 MHz*
COMMS-003	*The spacecraft shall send payload data to the Lunar Orbiter at frequency range 435-450 MHz*
COMMS-007	*The maximum available time limit for communication between the spacecraft and the Lunar Orbiter shall be 1 hour per day*
PDLPROC-01	*The payload processor shall receive and process a maximum 15 images per seconds from payload*
PDLPROC-02	*The payload processor shall store a maximum of 13 MB of payload data per 29 day period to the COMMS for transmission to Lunar Orbiter*
PDLPROC-03	*The payload processor shall interface with the payload on the Spacewire*

4.1 Propulsion

The trade-off related to the propulsion subsystem showed that chemical propulsion is the only feasible option for the main maneuvers (orbital transfer and station keeping), since all other options pose serious risks in terms of mass, volume and/or thrust level requirements. For the de-tumbling and de-saturation maneuvers, a clear preference should be given to a chemical or a cold gas system. The initial proposed design is based on a partially customized version of the VACCO Hybrid ADN MiPS, including one main mono-propellant thruster (ADN green propellant) providing a thrust of 0.1 N for the main maneuvers, plus four cold gas RCS thrusters in a "pyramid" configuration, providing a thrust of 10 mN each for the de-tumbling and de-saturation maneuvers. The preliminary design showed that the mission requirements can be accomplished with a system having a total wet mass of 5.6 kg and a total volume of 3.1U. Alternatives based on performing all required functions with the same propulsion type (mono-propellant or eventually resistojet), as well as systems based on completely European developments, are expected be investigated and better assessed during the next mission design phases.

4.2 Attitude Determination and Control

The preliminary architecture of the ADCS subsystem for LUMIO spacecraft is shown in Figure 7. The sensor suite has been chosen by selecting those with the smallest mass, volume and power budgets given the pointing requirements and potential tip-off rates.

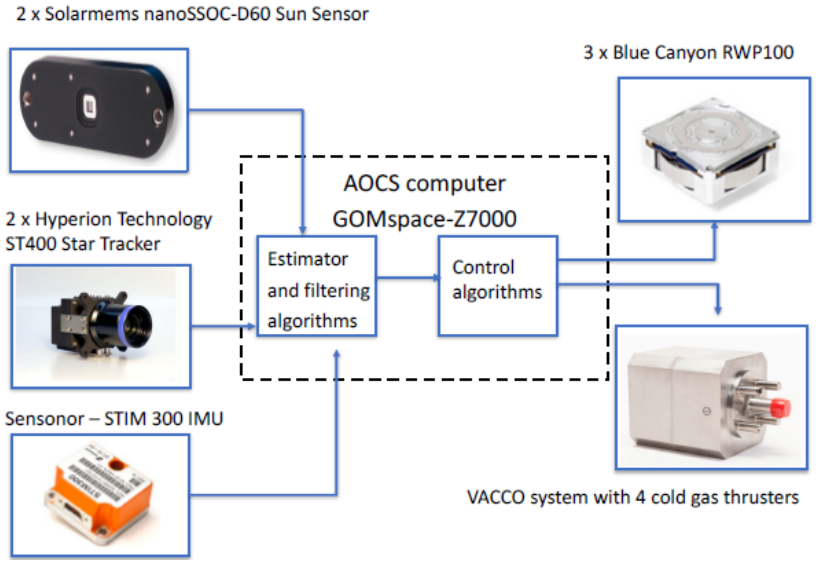

Figure 7. ADCS architecture of the LUMIO spacecraft

The sensor suite comprises a nano SSOC-D60 Sun sensor manufactured by Solar MEMs technology (43 x 14 x 5.9 mm, 6.5 g, accuracy of 0.5º 3σ and precision of 0.1º), two ST 400 star trackers manufactured by Hyperion Technologies and Berlin Space Technologies (53.8 x 53.8 x 90.5 mm, 280 g, accuracy of 10 arcsecs 3σ in pitch and yaw, and 120 arcsecs 3σ in roll axis), and a STIM 300 ultra-high performance inertial measurement unit manufactured by Sensonor10 (33 cm^3, 55 g). The on-board computer is the GOMspace-Z7000, also used for the navigation algorithm. The actuators comprise 3 Blue Canyon RWP-100 reaction wheels and the set of cold gas RCS thrusters included in the VACCO propulsion system. The Blue Canyon RWP-100 reaction wheels are assumed to operate at a maximum of 90 mNms despite their capability of 100 mNms momentum storage. The complete ADCS system has a mass of 2 kg and a volume of 1150 cm^3.

4.3 Power

For the solar array assembly, GOMSpace Nanopower MPS in its B-type configuration has been chosen, holding 16 AzurSpace 3G30C solar cell assemblies in its deployable configuration (currently under development). The size is 30 x 20 cm, with a thickness of 3.5 mm and a mass of 620 g inclusive of the solar cells. The deployable solar array is attached to a Solar Array Drive Assembly (SADA). The deployment of the solar array is achieved using a yoke which in turn is connected to the SADA inside the spacecraft. The total battery capacity is 160 Wh, achieved with two GOMSpace Nanopower BPX 80 Wh batteries.
For power conditioning and distribution, the GOMSpace Nanopower P60 unit has been selected. The interfaces between the EPS and the other subsystems are schematized in Figure 8. The total mass of the Electrical Power System is estimated at 2.9 kg.

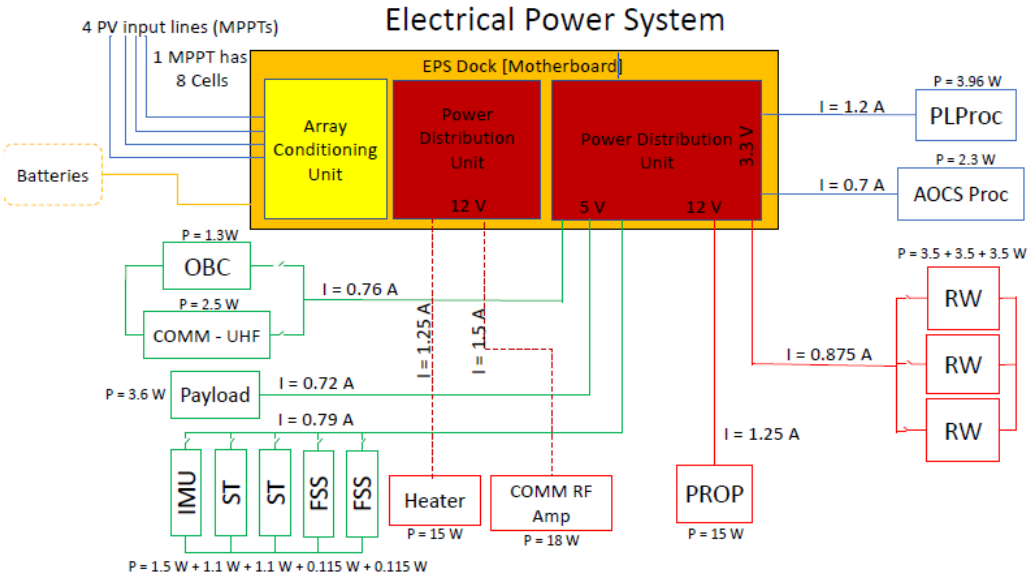

Figure 8. Electrical interfaces between the EPS and the other subsystems

4.4 Communication

The communication subsystem is based on two UHF turnstile antennas developed by ISIS-space (one for uplink and one for downlink, considering that the typical turnstile antennas bandwidth is less than 15 MHz in the UHF band) and a RF power amplifier allowing for an RF output power of 8W, necessary given the high transmission power required to close the link at large distances (75000 km). The UHF transponder is based on the Consultative Committee for Space Data Systems (CCSDS) Proximity-1 control, with RS442 data interface and a maximum data rate of 512 kbps. Table 10 shows the link budgets estimated for the current configuration of the Communications subsystem. In the operation phase, the PL/TM throughput is 25919 kB for a 29-day period with 16 one-hour communication slots. This means that, when the minimum payload data requirement of 12927 kB is met, the data budget available for telemetry is 12992 kB.

Table 10. Telemetry, Telecommand and Payload link budget

Link	TM return link	Payload data return link	TC Feeder link	Unit
Frequency	435	435	390	MHz
Modulation and coding	BPSK, Rate 1/2, K=7	BPSK, Rate 1/2, K=7	BPSK, Rate 1/2, K=7	-
Transmitter RF Power	8	8	2	W
Antenna (Gr/T)	-17.4	-7.8	-17.4†	-
Range	75000	75000	74400	km
Data Rate	1000	8000	1000	bps
Free Space Loss	182.7	182.7	181.7	dB
Received Eb/No	7.52	8.09	8.01	dB
Required Eb/No (BER=10^{-6})	5	5	5	dB
Margin	2.52	3.09	3.01	dB

† Conservative estimate since receiver details are not known. (Receiver at 60000 km from transmitter).

4.5 Structure and Thermal

The main satellite structure is a COTS-based 12U CubeSat structure produced by ISIS-space. A detailed radiation analysis has been conducted to define the thickness of the satellite external aluminium panels for sufficient radiation shielding, taking as a reference the LUMIO operational orbit and the position of the Moon for 1 year. SPENVIS's Solar particle model ESP-PSYCHIC (total fluence) was used to calculate the Total Ionizing Dose (TID) and long-term Single Event Upsets for the operational orbit. Then, using SHIELDOSE-2 model, the TID was plotted as a function of the thickness of aluminium shielding material of the spacecraft, see Figure 9. Since most of the internal spacecraft components can tolerate a TID up to 20 krad, and applying a 100% margin on this value due to the large uncertainties in this analysis, a thickness of 1.5 mm was selected, with additional internal shielding foreseen for particularly critical components (IMU, star trackers, SADA). The total mass of the structure designed with this criteria is 4 kg. The QuadPack deployer from ISIS-space is expected to be used for deploying the CubeSat from the Lunar Orbiter.

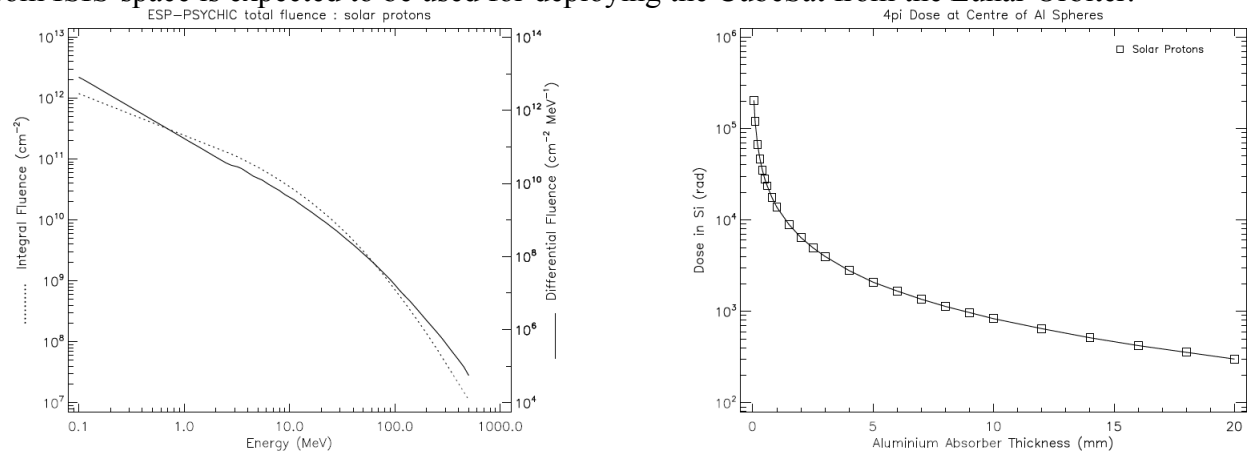

(a) Fluence Spectra. **(b)** Total Ionizing dose.

Figure 9. Radiation analysis for 1-y. near Earth interplanetary circular orbit of 435000 km radius, starting on 22/8/2023

A simplified steady state single node thermal analysis (with the main spacecraft body and the solar arrays considered as different thermally isolated bodies) has been conducted at this stage, given the still large uncertainties in the spacecraft internal and external design. Results showed that, with a combination of three different thermal coatings (27% gold, 25% silvered Teflon, 48% polished Al 6061-T6), spacecraft temperature is expected to stay in a range from -5 to +45 °C when illuminated by the Sun. In the few eclipse periods expected during the mission, much lower temperatures down to -50 °C were estimated, which might require the use of internal heaters for further thermal protection of the most critical components.

4.6 Command and Data Handling and Onboard Payload Data Processor

The selected OBC for the LUMIO spacecraft is the AAC Microtec Sirius computer, equipped with RS-422 and RS-485 connections as well as two SpaceWire 10 Mbps links, a 32-bit fault tolerant CPU and an EDAC protected memory. A CAN bus is foreseen for the connection with the ADCS and payload dedicated computers, as well as the Electrical Power System; although the selected computer does not support it natively, an option is available for accommodate a CAN-compatible transceiver upon request. The connection with the Communication subsystem is done with RS-422, the only type of link supported by the UHF transponder. For the dedicated Onboard Payload Data Processor, the GOMSpace Nanomind Z7000 processor has been selected. The OBPDP is connected to the camera through a SpaceWire interface, and to the main spacecraft OBC and dedicated ADCS computer through a CAN bus. This configuration allows for handling the required frame rate of 15 fps with a size of approximately 2 MB per frame.

4.7 Spacecraft Configuration

Figure 10 shows the current foreseen configuration for the LUMIO spacecraft, while the complete mass budget, including margins at system and subsystem level, is shown in Table 11. A total margined mass of approximately 21 kg is currently estimated for the spacecraft, well within the initial 24 kg requirement. The additional mass can be used for deviating from the zero-redundancy strategy by adding components to avoid single points of failure, for including additional propellant to extend the mission lifetime, or for accommodating additional payloads to exploit secondary mission objectives.

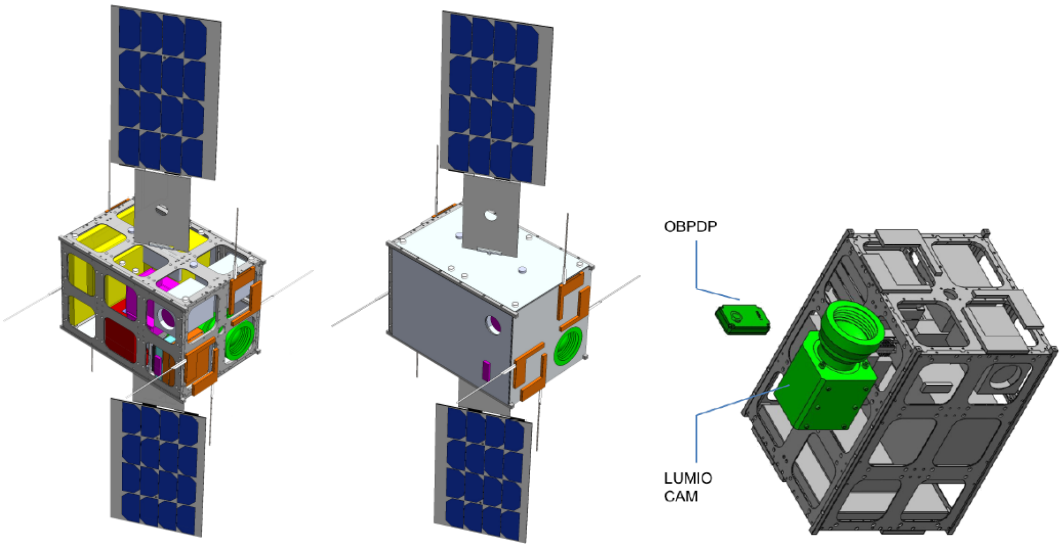

Figure 10. Complete LUMIO spacecraft without and with panels (left), and exploded view showing LUMIO-cam (right)

Table 11. Mass budget of the LUMIO spacecraft, including system and subsystem margins.

Component	Mass [kg]	Design approach	Subsystem Margin	Mass with margin [kg]
Payload	1.3	Custom Design	20%	1.56
Payload Processor	0.2	Full COTS	5%	0.21
Propulsion	5.585	COTS with modification	10%	6.1435
Communication	0.525	Custom Design	20%	0.63
CDHS	0.27	COTS with modification	10%	0.297
ADCS	1.994	Full COTS	5%	2.0937
EPS	2.862	COTS with modification	10%	3.1482
Structure	3.98	COTS with modification	10%	4.378
Thermal	0.135	COTS with modification	10%	0.1485
Electrical Harness	0.5	COTS with modification	10%	0.55
Total				19.1963
System margin			10%	
Total mass with system margin				21.07853

5 CONCLUSIONS

The primary science goal of LUMIO mission is to observe meteoroid impacts on the lunar farside in order to study the characteristics of meteoroids and to improve the meteoroid models. This might lead to a further study of the sources of these meteoroids, such as asteroids in the near-Earth environment and comets. The LUMIO mission complements ground-based observations with remote space-based observations, so improving the lunar situational awareness. The mission utilizes a 12U form-factor CubeSat which carries the LUMIO-Cam, an optical instrument capable of detecting light flashes in the visible spectrum to continuously monitor and process the data. The mission implements a novel orbit design and latest CubeSat technologies to serve as a pioneer in demonstrating how CubeSats can become a viable tool for deep space science and exploration.

LUMIO has been awarded winner (ex aequo) of ESA's LUCE (Lunar CubeSat for Exploration) SYSNOVA competition, and as such it is being considered by ESA for implementation in the near future. An independent assessment conducted at ESA's Concurrent Design Facility (CDF) has shown the mission feasible, and has identified possible delta-design options, which will be considered in the next phases of the mission design.

6 REFERENCES

[1] Z. Ceplecha *et al.*, "*Meteor Phenomena and Bodies,*" Sp. Sci. Rev., vol. 84, no. 3, pp. 327–471, 1998.

[2] P. Brown, R. E. Spalding, D. O. ReVelle, E. Tagliaferri, and S. P. Worden, "*The flux of small near-Earth objects colliding with the Earth.,*" Nature, vol. 420, no. 6913, pp. 294–296, 2002.

[3] J. L. Ortiz *et al.*, "*Detection of sporadic impact flashes on the Moon: Implications for the luminous efficiency of hypervelocity impacts and derived terrestrial impact rates,*" Icarus, 184, pp. 319–326, 2006.

[4] T. V Gudkova, P. H. Lognonné, and J. Gagnepain-Beyneix, "*Large impacts detected by the Apollo seismometers: Impactor mass and source cutoff frequency estimations,*" Icarus, vol. 211, no. 2, pp. 1049–1065, 2011.

[5] R. M. Suggs, D. E. Moser, W. J. Cooke, and R. J. Suggs, "*The flux of kilogram-sized meteoroids from lunar impact monitoring,*" Icarus, vol. 238, Supplement C, pp. 23–36, 2014.

[6] J. Oberst *et al.*, "*The present-day flux of large meteoroids on the lunar surface--A synthesis of models and observational techniques,*" Planet. Space Sci., vol. 74, pp. 179–193, 2012.

[7] S. Bouley *et al.*, "*Power and duration of impact flashes on the Moon: Implication for the cause of radiation,*" Icarus, vol. 218, no. 1, pp. 115–124, 2012.

[8] L. R. Bellot Rubio, J. L. Ortiz, and P. V Sada, "*Luminous Efficiency in Hypervelocity Impacts from the 1999 Lunar Leonids,*" Astrophys. J. Lett., vol. 542, pp. L65--L68, 2000.

[9] R. M. Suggs, W. J. Cooke, R. J. Suggs, W. R. Swift, and N. Hollon, "*The NASA Lunar Impact Monitoring Program,*" Earth. Moon. Planets, vol. 102, no. 1, pp. 293–298, 2008.

[10] A. Z. Bonanos *et al.*, "*NELIOTA: ESA's new NEO lunar impact monitoring project with the 1.2m telescope at the National Observatory of Athens,*" in *Proceedings of the International Astronomical Union*, 2015, vol. 10, no. S318, pp. 327–329.

[11] F. Topputo *et al.*, "*Lunar Meteoroid Impacts Observer.*" 2016.

[12] D. A. D. Tos and F. Topputo, "*On the advantages of exploiting the hierarchical structure of astrodynamical models,*" Acta Astronaut., vol. 136, pp. 236–247, 2017.

[13] D. A. Dei Tos and F. Topputo, "*Trajectory refinement of three-body orbits in the real solar system model,*" Adv. Sp. Res., vol. 59, no. 8, pp. 2117–2132, 2017.

[14] N. P. Dwivedi, "*Deterministic optimal maneuver strategy for multi-target missions,*" J. Optim. Theory Appl., vol. 17, no. 1, pp. 133–153, 1975.

[15] K. C. Howell and H. J. Pernicka, "*Stationkeeping method for libration point trajectories,*" J. Guid. Control Dyn., vol. 16, p. 151, 1993.

[16] K. Oguri *et al.*, "*EQUULEUS mission analysys: design of the science orbit phase,*" in *26th International Symposium on Space Flight Dynamics*, 2017, no. 72, pp. 1–7.

[17] V. Franzese, P. Di Lizia, and F. Topputo, "*Autonomous Optical Navigation for LUMIO Mission,*" in *2018 Space Flight Mechanics Meeting, AIAA SciTech Forum*, 2018, pp. 1–11.

[18] SRE-PA & D-TEC staff, "*Margin philosophy for science assessment studies,*" 2012.

[19] C. H. Acton Jr, "*Ancillary data services of NASA's navigation and ancillary information facility,*" Planet. Space Sci., vol. 44, no. 1, pp. 65–70, 1996.

[20] C. H. Acton Jr, N. Bachman, B. Semenov, and E. Wright, "*A look towards the future in the handling of space science mission geometry,*" Planet. Space Sci., vol. 150, pp. 9–12, 2018.